frontiers | Frontiers in Marine Science

TYPE Original Research
PUBLISHED 22 November 2024
DOI 10.3389/fmars.2024.1497453

OPEN ACCESS

EDITED BY
Haosheng Huang,
Louisiana State University, United States

REVIEWED BY
Guoxiang Wu,
Ocean University of China, China
Tao Wang,
Ocean University of China, China

*CORRESPONDENCE
Shasha Lu
lss003629@sio.org.cn

RECEIVED 17 September 2024
ACCEPTED 04 November 2024
PUBLISHED 22 November 2024

CITATION
Wang D, Lu S, Xie Z, Xia X and Liu Y (2024) High-resolution observations of longitudinal fronts in a well-mixed tidal channel. *Front. Mar. Sci.* 11:1497453. doi: 10.3389/fmars.2024.1497453

High-resolution observations of longitudinal fronts in a well-mixed tidal channel

Daoling Wang[1], Shasha Lu[1,2]*, Zhongyu Xie[1], Xiaoming Xia[1] and Yifei Liu[1]

[1]Second Institute of Oceanography, Ministry of Natural Resources, Hangzhou, China, [2]Key Laboratory of Ocean Space Resource Management Technology, Ministry of Natural Resources, Hangzhou, China

Longitudinal front is important for coastal dynamics, with crucial implications for sediment and pollutant transport. Three conventional theories have been proposed to explain the generation mechanisms of the longitudinal fronts. However, they are not completely supported by preliminary observation results within the Tiaozhoumen channel. Therefore, a field survey covering the whole flood-ebb tide, including high-resolution observations of velocity and density, was conducted to analyse the intra-tidal change of the fronts. The results showed that the fronts were mainly determined by the velocity shear, while the density gradient and Coriolis effect were small and negligible. Velocity structures presented significant differences between flood and ebb tides. Low velocity close to zero was present near the frontal zone at the flood tide. However, a velocity difference between shallow and deep bathymetry existed at the ebb tide. The flood fronts appeared longer and stronger than the ebb tide fronts. The fronts at ebb tide might be related to the velocity shear, due to differential bottom friction at varied depths from shallow to deep, consistent with the traditional theory of longitudinal front formation. The front system at flood tide is distinguished from the conventional fronts mentioned. The large Reynolds number and high turbulent dissipation rates in the frontal zone suggest that the fronts may be related to the boundary layer separation from the island. These findings provide evidence of the relationship between flood fronts and boundary layer separation; nonetheless, further studies must be conducted for a complete theory.

KEYWORDS

longitudinal front, tidal channel, observations, well-mixed, velocity shear

1 Introduction

Longitudinal fronts occurring in areas such as estuaries and tidal channels are frequently parallel to the estuarine axis or primary channel, and their existence has been recognised and documented for several years (Uncles, 2011). They are called "axial convergence fronts" in some studies (Huzzey and Brubaker, 1988) or "shear fronts" in others (O'Donnell, 1993). Longitudinal front is important for coastal dynamics, and has implications for sediment and pollutant transport required for coastal management (O'Donnell, 1998).

Three main theories have been proposed to explain the formation mechanisms of the longitudinal fronts. The first theory, frontogenesis, is associated with longitudinal density gradients and longitudinal flow with lateral shear (Huzzey and Brubaker, 1988). During flood tides, water in deep channels becomes more saline, compared with that in the shallow shoals, because of the high current velocity, thus creating a lateral pressure gradient directed towards the deeper and shallow sides at the surface and bottom, respectively. This gradient causes the surface water to converge, leading to the formation of fronts. These convergence fronts are usually recognised by surface signatures such as a line of foams and debris or slick. During ebb tides, divergence replaces surface convergence. In this scenario, a density gradient is a necessary condition for frontogenesis. However, the density difference in our study channel may be very small. In previous study, the densities of the flood and ebb current in the study channel were approximately 1018.86 and 1018.24 kg m^{-3}, respectively (Lu et al., 2017).

Second, under scenarios of no or minimal density differences, longitudinal fronts may occur owing to tidal convergences, associated with frictional tide and bathymetry (Li et al., 2001; Lu et al., 2020). Due to frictional differences between deep and shallow waters, a significant change in the across-channel velocity occurs across bathymetry changes (Li et al., 2001; Li, 2002). The differential velocities result in differential rotations of tidal ellipses, generating convergence and divergence at different tidal stages. In our study channel, visual observation showed that the surface signature of the fronts appeared during flood tide, indicating a surface convergence at that time. However, velocity shear at maximum flood tide usually induces surface divergence, which is inconsistent with the observed results.

Third, longitudinal fronts can be generated by a combination of Coriolis force and lateral boundaries (Mied et al., 2000). Due to strong bottom friction, a horizontal vorticity is caused by the tilt of the vertical planetary vortex. A net vortex associated with the boundary of the channel and a transverse flow is formed, generating a longitudinal front.

Based on the above preliminary results, the longitudinal fronts that occurred in our study channel are not completely supported by the three traditional frontogenesis. To gain insight of the underlying causes of longitudinal fronts, a field survey covering a whole flood-ebb tide was conducted to measure three-dimensional current velocity, temperature, and salinity on repeated transects across the frontal zone during front presence and absence.

2 Materials and methods

2.1 Study area

The study area is situated in the Tiaozhoumen channel between the islands of Liuheng and Xiazhi, south of the Zhoushan Archipelago (Figure 1A). The tide in the Tiaozhoumen channel reaches a monthly peak of 4.5 m and an average of 2.3 m. The wave is weak, with an average annual height of 0.4 m. During our field observations, the sea was relatively calm, with no large waves. The channel demonstrates a rotating flow in the southeast and a reciprocating flow in the centre and northwest. The fronts appeared in the centre channel, where the flow velocity can reach up to approximately 2.57 m/s (Zhou, 2010). Numerous islands and reefs exist in the southeast of the Tiaozhoumen channel. The flood current is blocked by the Yuanshan and Liangtan islands and divided into several branches entering the channel (Figure 1A).

Frontal surface lines marked by slick were visually observed during the flood tide (Figure 1B) from 25 May to 1 June in 2015 and 7 February to 7 April in 2023. They were parallel to the primary channel and/or depth contours. The profile topography perpendicular to the frontal lines is illustrated in Figure 1C (Acoustic Doppler current profiler (ADCP) Transect-2015 in Figure 1A). There were two slopes, one from 8 to 15 m, the other from 15 to ≥ 20 m.

2.2 Data collection

Based on the visibility of the frontal surface line, two field surveys with transects perpendicular to the frontal surface line were set up to capture the front and measure the frontal structure in 2015 and 2023 (Figure 1A).

In 2015, a repeated observation of velocity and density was performed between 05:33 and 17:22 on 1 June (all times are Beijing local time, UTC _08:00; Figure 2), with approximately a 13-h window covering an entire flood-ebb tidal period. A fixed-point ADCP collected the flow velocity data with continuous mode (the location was shown in Figure 1A), which indicates that the flood tide occurred between 05:00 and 10:30 and the ebb tide occurred between 10:30 and 17:00 (Figure 2). Overall, 13 transects were measured (black line in Figure 1A, labelled as ADCP Transect-2015), with approximately one transect measured every hour. Every transect collected velocity data on a going way from shallow to deep (each ADCP survey in one transect was performed after approximately 15 min, Grey shadings T1–T13 in Figure 2) and the density data were collected on a back way (three samples in each transect). The velocity data were collected using ADCP 600 kHZ downward-looking, vessel-mounted, and continuous logging. Thirteen sets of ADCP transects (T1–T13) were observed along the survey line (black line as shown in Figure 1A). The vertical resolution was set to 1 m. The horizontal resolution was approximately 0.4 m, as estimated from a vessel speed of four knots and a sampling frequency of 1.3 Hz. The density data

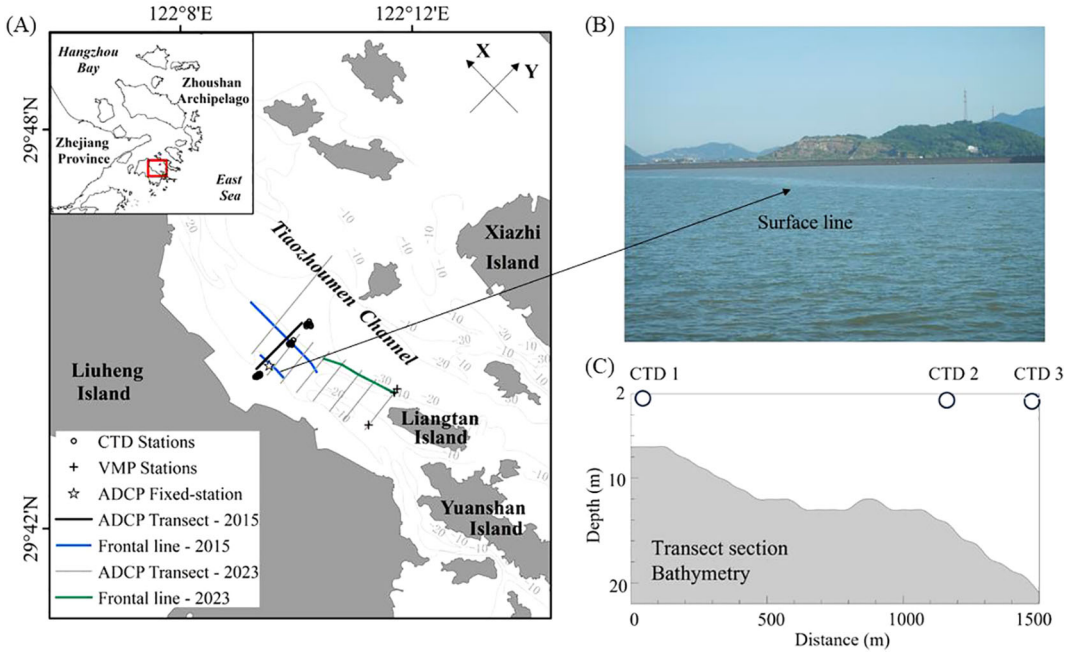

FIGURE 1
(A) Map of the Tiaozhoumen channel. Acoustic Doppler current profiler (ADCP) Transect-2015 (black line) was repeatedly measured over a 13-h period on 1 June, 2015. Light blue lines indicate the visible surface lines recorded in 2015. ADCP Transect-2023 (grey lines) was measured once to record the frontal line (green line) in 2023. VMP stations sampled synchronously. **(B)** Photograph of the Tiaozhoumen channel frontal surface line captured on 1 June, 2015. **(C)** Profile terrain for the ADCP Transect-2015. CTD2 is situated within the surface line area, while CTD1 and CTD3 are located on the shallow and deep sides of the surface line, respectively.

were collected using conductivity-temperature-depth (CTD). The average depth resolution and sampling time frequency were approximately 0.1 m and 6 HZ, respectively. Overall, 37 sampling stations were measured to collect vertical profiles of water temperature, salinity, and turbidity, via a CTD lifted by a hand-operated winch. The dense station's positions were set as three areas representative of the (1) shallow side of the frontal zone (considered CTD1 in Figure 1C), (2) frontal zone (considered CTD 2 in Figure 1C), and (3) deep side of the frontal zone (considered CTD3 in Figure 1C). Owing to uncontrollable factors in the field survey, CTD2 vertical profile data could not be obtained for T8 and T13.

Further, the frontal line was recorded through the onboard Differential Global Positioning System (GPS) recording real-time latitude and longitude of the vessel. The vessel navigated along the frontal line; thus, the vessel navigation was the observed front line. This type of mapping of the front shape was performed on 27 and 31 May, 2015 (blue lines in Figure 1A). In our survey, the recorded times for the front were uncoordinated, resulting in an error in front positions. The rate of the front lateral migration was roughly 45 m h^{-1}, with a maximum migration distance of 200 m for 4.5 h by the repeated records in 2015. Therefore, front position error due to different record timing (no more than 1 h) would be less than 45 m and could be disregarded.

Repeated observations over a period of 13 h in 2015 provided detailed data on frontal velocity and density structures between the flood and ebb tide. However, the shape record of the front may not be complete, because the existence of the front has a time limit. That

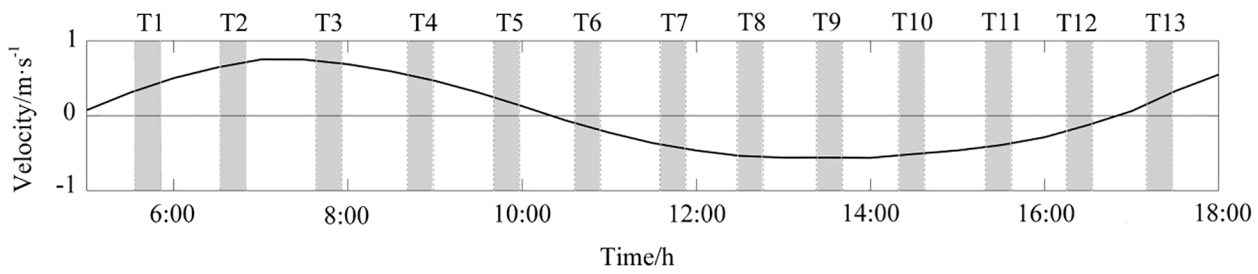

FIGURE 2
Schematic of the observation period on 1 June, 2015. The black solid line represents the velocity of the tidal current flow measured at the fixed-point ADCP. Grey shadings (T1–T13) represent the transect ADCP surveying time.

is, the recorded location where the front disappeared in 2015 may be due to the disappearance over time, rather than the end of the front shape. Based on a preliminary analysis of the 2015 data, we found that the front was strongest at the time of maximum flood and it was likely triggered by the Liangtan Island. Therefore in 2023, a field survey was conducted to confirm the complete frontal shape in the study area, through seven sections in the downstream direction behind the Linagtan Island during flood peak. The vessel navigated across the frontal line, and the timing of each encounter of the visible front was recorded. By comparing the recorded timing with the vessel's GPS record, the positions of the observed front were recorded. Five positions of fronts recorded in 2023 were connected to form the complete frontal shape (green line in Figure 1A). Besides, turbulence data in and out of the frontal zone were collected using a turbulence profiler (TurboVMP) by hand-lifted in 2023.

2.3 Velocity data processing

MATLAB was used to process the flow velocity data collected on 1 June, 2015. A new x and y coordinate system was specified according to the frontal direction (Figure 1A). The x-direction was oriented along the front (perpendicular to the transect), which was denoted by the current velocity component u, with a positive direction aligned with flooding; the y-direction was oriented across the front (along the transect), which was denoted by the current velocity component v, with a positive direction aligned offshore. The impact of vessel speed on flow velocity measurements was eliminated using bottom tracking mode. The ADCP survey transect profile data were averaged at 10-s intervals to remove heading errors and noise, which were then converted to geographic coordinates and finally converted to the new coordinate system. Each individual 10-s ensemble represents an average value over a horizontal distance of approximately 20 m at a vessel speed of approximately 2 m s^{-1}.

3 Results

3.1 Preliminary observations

The observed fronts were usually longitudinal along the depth contour, based on the vessel mapping in Figure 1A. The positions were situated in the two sloping areas, at depths of approximately 9 ± 1 m and 15 ± 1 m. The width of the frontal line was several metres. According to the description of the locals and the observed results, the front could extend as far as the Liangtan Island. In addition, the visible observed front appeared only at flood tide, also indicated by the 13-h observational results on 1 June, 2015, with the front initially observed at approximately 5:30 a.m. and disappearing at 10:00 a.m.

During the day, the density differences in our observational region were extremely small, both vertically (± 0.17, ± 0.24, and ±0.23 kg m^{-3} for the CTD1, CTD2, and CTD3 averages, respectively) and horizontally (± 0.03 kg m^{-3} from CTD1 to CTD2 average, and ±0.08 kg m^{-3} from CTD2 to CTD3 average). The maximum difference in salinity was 0.35 PSU in the horizontal front, considerably smaller than that in other fronts (0.8–1 PSU) (Sarabun, 1980; Nunes and Simpson, 1985; Huzzey and Brubaker, 1988). It is therefore clear that the observed fronts in this study were not caused by density gradient; that is, the front system is related to velocity shears.

3.2 Velocity

As the surface line is only one representation of a front, the absence of such lines does not necessarily imply that fronts are non-existent (Largier, 1993). Therefore, fronts are typically identified using the gradient method, which enables the recognition of fronts that lack significant surface representation (Tang, 1996). In this study, the density gradient was negligible. The flow velocity along the front (u) was considerably greater than that across the front (v). Therefore, the longitudinal velocity shear $\partial u/\partial y$ was used as an index for front discrimination.

As T13 marked the beginning of the next flood tide (Figure 2), the flow velocity map of the T13 section was placed before T1, considering the coherence in the analysis of flood and ebb tidal velocities. The along-front velocity (u) and the transverse shear of the along-channel velocity ($\partial u/\partial y$) exhibited two distinct distribution characteristics at flood and ebb tides.

During a flood tide, most sections exhibited a strip-like low-velocity zone of u with a width of approximately 100 m in the sloping area (Figure 3A). T13–T3 represented the transition period from the flood beginning to the maximum flood. The along-front velocity (u) on the deep channel and shallow shoal had similar values, increasing from 0.1 to 0.9 m/s. At T1, a strip-like zone of low velocity, where u approaches zero, was initially observed at a position of 1,100–1,200 m. At T2, a new strip-like zone of low flow velocity appeared at approximately 200–300 m. Between T3 and T5, a shift from maximum flood to flood slack occurred, decreasing the flood velocity from 0.9 to 0.3 m/s. The low-velocity zone close to the deep side persisted, while the one close to the shallow side disappeared at T5. For T1–T5, the low-velocity zone migrated toward the deeper side for approximately 200 m.

During the ebb tide, the distribution characteristics of the u section differed from those during the flood tide (Figure 3A). The most significant difference was that the low-velocity zones disappeared, and a velocity difference appeared between the shallow shoal and deep channel. At the start of the falling tide (T6), the u component of the entire section approached zero. From T7 to T9, an increase in the velocity of the ebb tides was observed. The u average of the shallow shoal increased from -0.48 to -0.87 m/s, while the u average of the deep side increased from -0.57 to -1.12 m/s. Furthermore, the velocity difference between the two water bodies gradually increased from 0.09 to 0.25 m/s. From periods T9 to T12, the u section on the shallow shoal decreased from -0.87 to -0.46 m/s, and that on the deep side decreased from -1.12 to -0.53 m/s. The velocity difference between the two sides decreased from 0.25 to 0.07 m/s.

In our study, the longitudinal velocity shear $\partial u/\partial y$ was used as an index for front discrimination. A previous study (Liu, 2009) reported the critical value of the velocity gradient to be 0.004 s^{-1};

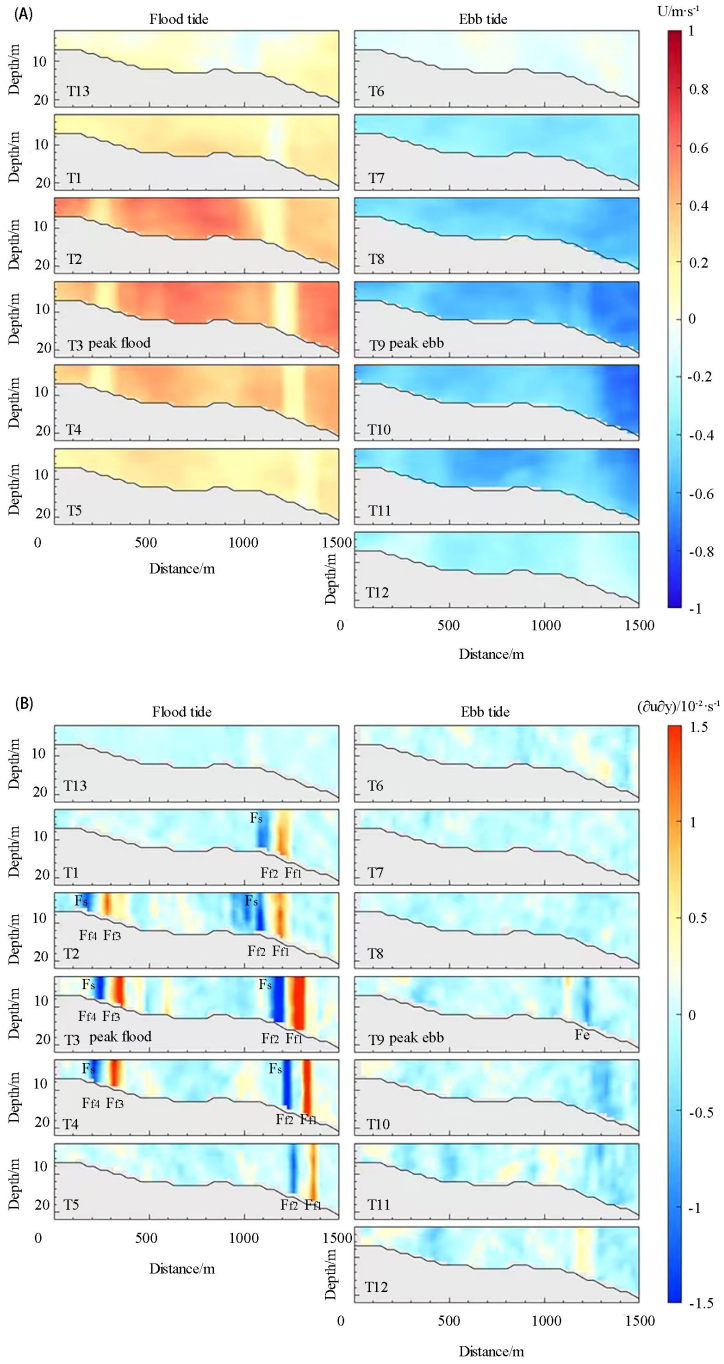

FIGURE 3
(A) Along-front components (u) for each repetition of the ADCP Transect-2015. **(B)** Across-front gradient of the along-front velocity ($\partial u/\partial y$) for each repetition of the ADCP Transect-2015. u is a positive direction aligned with flooding.

that is, the velocity shear $|\partial u/\partial y| > 0.004\ s^{-1}$ was recognised as a front. Here, during flood tide, four fronts were observed, namely F_{f1}, F_{f2}, F_{f3}, and F_{f4}, while the visible fronts namely F_s (Figure 3B) were observed. F_{f1}/F_{f2} and F_{f3}/F_{f4} in each transect occurred in pairs. Both fronts in each pair exhibited similar intensities but in reverse directions. The intensities of all fronts varied with the tide. During early to maximum flood (T13–T3), F_{f1} and F_{f2} first appeared at the moment of T1, and the frontal intensity ($|\partial u/\partial y|$) increased from 0.006 to 0.014 s^{-1} from T1 to T3. Furthermore, F_{f3} and F_{f4} first appeared at the moment of T2, and the frontal intensity ($|\partial u/\partial y|$) increased from 0.007 to 0.009 s^{-1} from T2 to T3. During maximum flood-to-flood slack (T3–T5), F_{f1} and F_{f2} were consistently present, although F_{f3} and F_{f4} disappeared at T5. The frontal intensity of F_{f1}/F_{f2} gradually decreased from 0.014 s^{-1} to 0.006 s^{-1} between T3 and T5, whereas that of F_{f3}/F_{f4} gradually decreased from 0.009 to 0.008 s^{-1} between T3 and T4. The front

during the flood was the most intense at T3. During ebb tide, the front F_e only occurred at the peak ebb T9, with $|\partial u/\partial y|$ =0.005 s^{-1} (Figure 3B).

To quantitatively evaluate cross-frontal flow convergence or divergence, the across-front gradient of the across-front velocity ($\partial v/\partial y$) was used as an indicator, whose negative, positive, and absolute values denote convergence, divergence, and convergence (or divergence) strength, respectively (Framiñan et al., 2008). Thus, two typical transects with the strongest frontal intensity of flood peak T3 and ebb peak T9 were selected to calculate $\partial v/\partial y$ (Figure 4). The flood front F_{f2} and F_{f4} were convergent with $\partial v/\partial y = -0.84$ (10^{-2} s^{-1}) and -0.98 (10^{-2} s^{-1}), while the flood front F_{f1} and F_{f3} were divergent $\partial v/\partial y = 0.72$ (10^{-2} s^{-1}) and 0.29 (10^{-2} s^{-1}), and the ebb front F_e was divergent $\partial v/\partial y = 0.74$ (10^{-2} s^{-1}). This finding confirms that no front signatures were observed at the ebb tide and two front lines were observed at the flood tide. The surface line indicated a surface convergence. The positions of convergence fronts F_{f2} and F_{f4} during flood tide were consistent with the visible front lines.

4 Discussion

4.1 Bottom friction and difference in water depth

Salinity gradient or velocity shear is a dynamic factor that triggers the oceanic front generation. We found that the salinity gradients herein were weak and negligible. The transverse velocity shear ($\partial v/\partial y$) revealed that the velocity shear was enhanced in the frontal zone, while that of the non-frontal zone was close to zero (Figure 4). Thus, velocity shear in the barotropic environment was found to be the main mechanism underlying longitudinal front generation in this study.

Velocity shear can be generated by the differences in water depth through friction effects (Brown and Davies, 2010; Li, 2002). This theory is supported by observations (Li and Valle-Levinson, 1999) and analytical models (Li, 2001). Based on the topography profile (Figure 1), differences were noted in water depth in our study on either sides of the front. An optimal estimate of the bottom drag coefficient (representing the friction effect) as a function of the water depth was provided by Li and Valle-Levinson, 1999. In our channel, the water depth varied from approximately 12 m in the shallow shoal to 20 m in the deep side (Figure 1C). The corresponding drag coefficients varied from 0.0026 to 0.0020. The increase in drag coefficients in a shallow channel results in a decrease in velocity, compared with that in the deep side. A difference in the flow velocity of approximately 0.25 m/s between the two sides of the front F_e and a transverse velocity shear of approximately 0.74 (10^{-2} s^{-1}) at the frontal zone were observed at the peak ebb T9 (Figures 3 and 4). Therefore, unequal tidal velocities caused by the difference in water depth between the shallow and deep channels through friction effects might generate the longitudinal shear front at ebb tide.

In addition, the calculated absolute value of the shear velocity was 10^{-3} s^{-1} of frontal zone, much larger than that of the planetary vorticity at 10^{-4} s^{-1}, by one order of magnitude. Therefore, Coriolis force is unimportant in generating the longitudinal shear fronts in the tidal channel, consistent with our expectations. The third mechanism for longitudinal front generation is excluded in the study. Besides, velocity distribution at flood tide presented a low-velocity characteristic in the sloping area, instead of velocity differences at varied depths. It is implied that there may be other mechanisms for the generation of the fronts.

4.2 Boundary layer separation from island

Velocity shear can be generated by boundary layer separation from an abrupt topographic change (McWilliams, 2021). A conspicuous example is bottom fronts at the topographic shelf-slope boundary (Chapman, 2000). Furthermore, the fronts were observed as flow separating from a nearby island or headland (Geyer and Signell, 1990; Molemaker et al., 2015). However, this argument is rarely mentioned in coastal front reviews (O'Donnell, 1993; Uncles, 2011); therefore, it was not mentioned as a typical frontogenesis mechanism in the introduction.

The survey of complete frontal shape in 2023 revealed that the front at flood tide generates from the Liangtan Island (Figure 1A). Field observations by Farmer et al. (2002) showed that the flow structure at the shear layer (i.e. the position of the front) was characterised by an along-front velocity close to zero, which is consistent with the flow structure of the frontal zone in our study (Figure 3). Therefore, the shape and structure of the front suggest that the fronts appearing during flood tide are related to the boundary layer separation from the island.

According to the theory of flow separation, when currents encounter an isolated island, the boundary stresses associated

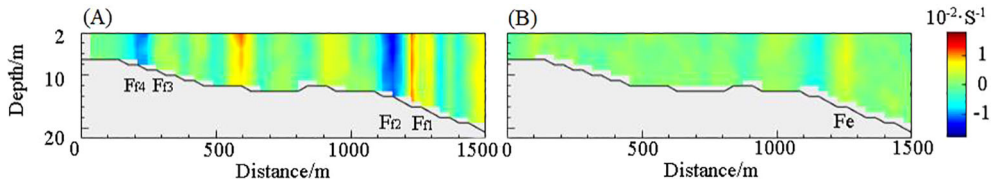

FIGURE 4
Across-front gradient of the across-front velocity $\partial v/\partial y$ at **(A)** maximum flood T3 and **(B)** maximum ebb T9.

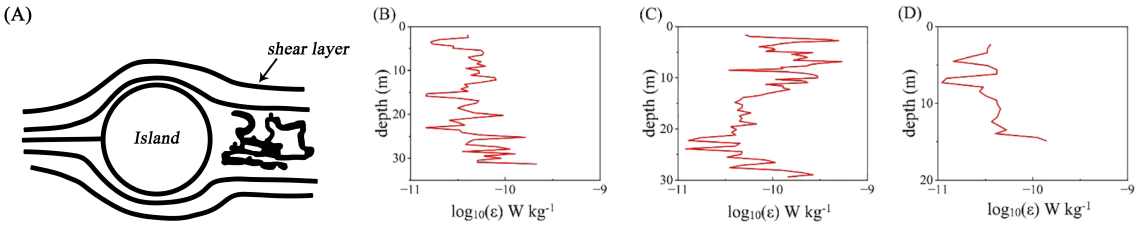

FIGURE 5
(A) Schematic diagram of shear layer downstream of an island at *Re* = 1666. **(B)** Distribution of turbulent dissipation rates at the deep side station of the front. **(C)** Distribution of turbulent dissipation rates at the frontal station. **(D)** Distribution of turbulent dissipation rates at the shallow side station of the front. The station's positions are labelled in Figure 1A marked by '+'. The shear layer in the schematic diagram is the frontal zone.

with the nearshore or lateral side of the island cause strong boundary shear flow (Teinturier et al., 2010). Reynolds number (*Re*) is critical for the flow separation. The wake downstream presents a different nature with the increase in *Re* (Tritton, 1988). The calculation of *Re* is as follows,

$$Re = \frac{Ul}{m}$$

where U represents the upstream flow velocity, l denotes the characteristic length (in this case it is the width of the Liangtan Island), and m denotes the horizontal eddy viscosity. The eddy viscosity (m) is 10 orders of magnitude greater than the molecular viscosity in the real marine environment; thus, it is more commonly used when considering island wakes. Values of eddy viscosity based on many experimental determinations increase with the length scale of interest l in a nonlinear fashion $m = 2.2{\star}10^{-4}l^{1.13}$ (Barton, 2001). Thus, substituting U at maximum flood tide on 1 June, 2015 (0.9 m s^{-1}) and l (1000 m) into the equation, *Re* was calculated to be 1666. According to Tritton (1988), when $Re > 1000$, the separation flow downstream of the cylinder may become turbulent and extend downstream with the current (Figure 5A).

It is also supported by our observations of turbulent dissipation rates between O(10^{-9}–10^{-10}) W kg^{-1} at surface of the frontal zone (e.g. the shear layer), much larger than that at the non-frontal region between O(10^{-10}–10^{-11}) W kg^{-1} by one order of magnitude (Figures 5B–D). The high turbulent dissipation rate can lead to average flow energy transfer to small-scale turbulence, which explain the low velocity in the frontal zone during flood tide. Therefore, there findings suggest that the fronts appeared during flood tide may be related to the boundary layer separation from the island. The large Eddy Simulation model is an efficient tool for simulating such a front. In the model, different *Re* can be numerically simulated to analyse the corresponding relationship between frontogenesis and *Re*.

4.3 Influence on sediment transport

Estuarine density fronts are known as sieves or sinks that trap sediment and various pollutants (Largier, 1993). The trap mechanisms have been extensively studied, the most important of which is the change in salinity from land to sea in estuaries. When fresh water and more ionic seawater meet, enhanced deposition may be expected at the front owing to the flocculation of fine particles (Largier, 1993).Therefore in the regine of estuarine density fronts, sediment deposition often occurs resulting in topographic changes

However, the water in the Tiaozhoumen channel in this study is well mixed, indicating the absence of trap effect of the estuarine front on the sediment. To understand the influence of the longitudinal front on the sediment transport, the suspended sediment concentrations (SSC) in the frontal area and the non-frontal area were compared, and the moment T3 of the strongest front was selected. The results revealed that the SSC in the frontal zone was significantly higher than that on both sides at water depths of 5–15 m (Figure 6). According to the study of sediment and turbulent mixing, the increased turbulence would resuspend the sediment and increase the SSC (Luo et al., 2017; Qiu et al., 2017). The presence of longitudinal fronts increases the turbulent mixing,

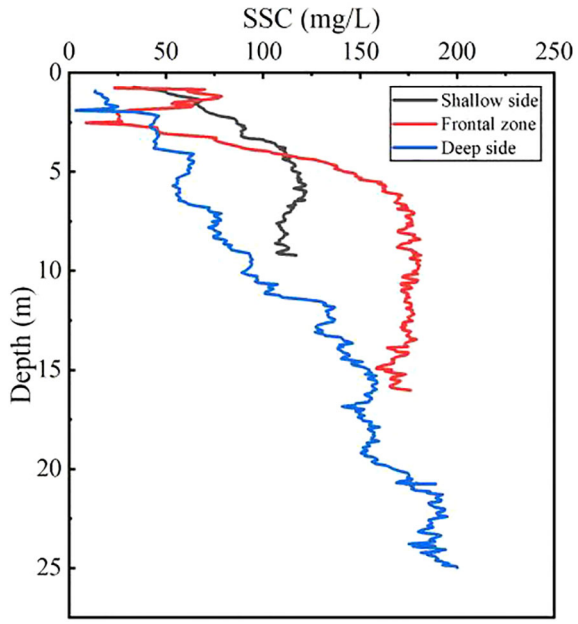

FIGURE 6
Vertical profiles of SSC in the frontal zone and shallow/deep sides at the maximum flood T3.

leading to the vertical motion of sediment and increased SSC. However, the longitudinal front does not consistently persist as estuarine density fronts. Its influence on the topography would be linked to the sediment sources and corresponding tidal patterns. The morphological evolution under the impact of the longitudinal front would be further researched in subsequent studies.

5 Conclusions

Longitudinal fronts were observed along the Tizaozhoumen channel. The positions of the fronts were relatively stable at the slope from shallow to deep. In the study region, the density differences were extremely small vertically and horizontally, suggesting that the front was formed without a density gradient. The velocity shear was at least one order of magnitude larger than the planetary vorticity, suggesting the negligible Coriolis effect.

The velocity structure and shear across the frontal zone presented significant differences between the flood and ebb tides. During the ebb tide, a velocity difference existed at the slope between the shallow and the deep, probably caused by differential bottom friction. The mechanism of frontal generation was similar to that observed for conventional shear fronts. During flood tide, low-velocity zones existed near the frontal zone. The flood fronts appeared longer and stronger than the ebb tide. The front system at flood tide was distinguished from the conventional fronts and may be related to the boundary layer separation from the Liangtan Island; further, owing to Reynolds number at maximum flood tide being large, the separation flow became turbulent. This was also supported by the observed data on turbulent dissipation rates. The Reynolds number and turbulent dissipation rates during flood tide only provide evidence for the relation of the fronts and boundary layer separation from the island. Large Eddy Simulation model would be required for further research in the future.

Additionally, the convergence and divergence of the velocity were calculated and compared with the front positions. The ebb fronts were divergent and the flood fronts were half convergent and half divergent. The convergence fronts were consistent with the observed frontal line marked by slick change.

Data availability statement

The original contributions presented in the study are included in the article/supplementary material, further inquiries can be directed to the corresponding author.

Author contributions

SL: Conceptualization, Funding acquisition, Writing – review & editing. DW: Data curation, Formal analysis, Visualization, Writing – original draft. ZX: Investigation, Validation, Writing – review & editing. XX: Project administration, Resources, Supervision, Writing – review & editing. YL: Investigation, Writing – review & editing.

Funding

The author(s) declare that financial support was received for the research, authorship, and/or publication of this article. This study was supported by the National Natural Science Foundation of China (grant numbers 41406099 and 42376153) and the Scientific Research Fund of the Second Institute of Oceanography, Ministry of Natural Resources (grant no. SZ2302).

Acknowledgments

We thank Cao Zhenyi and Cai Tinglu for their assistance with fieldwork, Prof. Li Yan for his guidance in drafting the paper, Shen Siyuan and Yang Bowen for their assistance with drawings. We thank Editage (www.editage.cn) for providing language assistance. An earlier version of this paper was presented at the 2024 6th International Conference on Geoscience and Remote Sensing Mapping.

Conflict of interest

The authors declare that the research was conducted in the absence of any commercial or financial relationships that could be construed as a potential conflict of interest.

Publisher's note

References

Barton, E. D. (2001). "Turbulence and diffusion: island wakes," in *Encyclopedia of ocean sciences*, Academic Press, United State. 1397–1403. doi: 10.1006/rwos.2001.0140

Brown, J. M., and Davies, A. G. (2010). Flood/ebb tidal asymmetry in a shallow sandy estuary and the impact on net sand transport. *Geomorphology*. 114, 431–439. doi: 10.1016/j.geomorph.2009.08.006

Chapman, D. C. (2000). Boundary layer control of buoyant coastal currents and the establishment of a shelfbreak front*. *J. Phys. Oceanogr.* 30, 2941–2955. doi: 10.1175/1520-0485(2001)031<2941:BLCOBC>2.0.CO;2

Farmer, D., Pawlowicz, R., and Jiang, R. (2002). Tilting separation flows: a mechanism for intense vertical mixing in the coastal ocean. *Dynam. Atmos. Oceans.* 36, 43–58. doi: 10.1016/S0377-0265(02)00024-6

Framiñan, M. B., Valle-Levinson, A., Sepúlveda, H. H., and Brown, O. B. (2008). Tidal variations of flow convergence, shear, and stratification at the Rio de la Plata estuary turbidity front. *J. Geophys. Res.* 113, C08035. doi: 10.1029/2006JC004038

Geyer, W. R., and Signell, R. (1990). Measurements of tidal flow around a headland with a shipboard acoustic Doppler current profiler. *J. Geophys. Res. Oceans (Geyer: W.R. Ralston: D.K.). Estuar. frontogenesis.* 95, 3189–3197. doi: 10.1029/JC095iC03p03189

Huzzey, L. M., and Brubaker, J. M. (1988). The formation of longitudinal fronts in a coastal plain estuary. *J. Geophys. Res.* 93, 1329–1334. doi: 10.1029/JC093iC02p01329

Largier, J. L. (1993). Estuarine fronts: how important are they? *Estuaries.* 16, 1–11. doi: 10.2307/1352760

Li, C. (2001). 3D analytic model for testing numerical tidal models. *J. Hydraul. Eng.* 127, 709–717. doi: 10.1061/(ASCE)0733-9429(2001)127:9(709

Li, C. Y. (2002). Axial convergence fronts in a barotropic tidal inlet—sand shoal inlet, VA. *Contin. Shelf Res.* 22, 2633–2653. doi: 10.1016/S0278-4343(02)00118-8

Li, G. X., Tang, Z. S., Yue, S. H., Zhuang, K., and Wei, H. (2001). Sedimentation in the shear front off the Yellow River mouth. *Contin. Shelf Res.* 21, 607–625. doi: 10.1016/S0278-4343(00)00097-2

Li, C., and Valle-Levinson, A. (1999). A two-dimensional analytic tidal model for a narrow estuary of arbitrary lateral depth variation: the intratidal motion. *J. Geophys. Res.* 104, 23525–23543. doi: 10.1029/1999JC900172

Liu, C. Y. (2009). Distributions and intra-seasonal evolutions of the sea surface thermal fronts in the Yellow Sea warm current origin area (in Chinese). *Mar. Sci.* 33:87–93.

Lu, S. S., Xia, X. M., Cao, Z. Y., Liu, J., Thompson, C. E. L., and Cai, T. L. (2020). High-resolution observations of a shear front in a tidal channel. *Estuar. Coast. Shelf Sci.* 232, 106521. doi: 10.1016/j.ecss.2019.106521

Lu, S. S., Xia, X. M., Thompson, C. E. L., Cao, Z. Y., and Liu, Y. F. (2017). Observations of a tidal intrusion front in a tidal channel. *Estuar. Coast. Shelf Sci.* 198, 12–20. doi: 10.1016/j.ecss.2017.08.030

Luo, Z., Zhu, J., Wu, H., and Li, X. (2017). Dynamics of the sediment plume over the Yangtze Bank in the Yellow and East China Seas. *JGR Oceans.* 122, 10073–10090. doi: 10.1002/2017JC013215

Mied, RP, Handler, RA, and Evans, TE (2000). Longitudinal convergence fronts in homogeneous rotating channels. *JGR-oceans.* 105, 8647–8658.

McWilliams, J. C. (2021). Oceanic frontogenesis. *Annu. Rev. Mar. Sci.* 13, 227–253. doi: 10.1146/annurev-marine-032320-120725

Molemaker, M. J., McWilliams, J. C., and Dewar, W. K. (2015). Submesoscale instability and generation of mesoscale anticyclones near a separation of the California Undercurrent. *J. Phys. Oceanogr.* 45, 613–629. doi: 10.1175/JPO-D-13-0225.1

Nunes, R. A., and Simpson, J. H. (1985). Axial convergence in a well-mixed estuary. *Coast. Shelf Sci.* 20, 637–649. doi: 10.1016/0272-7714(85)90112-X

O'Donnell, J. (1993). Surface fronts in estuaries: a review. *Estuaries.* 16, 12–39. doi: 10.2307/1352761

O'Donnell, J., Marmorino, G. O., and Trump, C. L. (1998). Convergence and downwelling at a river plume front. *J. Phys. Oceanogr.* 28, 1481–1495. doi: 10.1175/1520-0485(1998)028<1481:CADAAR>2.0.CO;2

Qiu, C., Su, D. Y., Mao, H. B., Wu, J. X., Cui, Y. S., and Wang, D. X. (2017). Observational evidence for turbulent effects on total suspended matter within the Pearl River plume. *Contin. Shelf Res.* 151, 15–22. doi: 10.1016/j.csr.2017.10.001

Sarabun, C. C. (1980). Structure and formation of Delaware Bay fronts [Ph.D. dissertation]. The University of Delaware, Newark, DE, 229.

Tang, Y. X. (1996). *Distributional features and seasonal variations of temperature fronts in the east China sea (in Chinese)* (Oceanologia Limnologia Sin), 27, 436–444.

Teinturier, S., Stegner, A., Didelle, H., and Viboud, S. (2010). Small-scale instabilities of an island wake flow in a rotating shallow-water layer. *Dynam. Atmos. Oceans.* 49, 1–24. doi: 10.1016/j.dynatmoce.2008.10.006

Tritton, D. J. (1988). *Physical fluid dynamics* (Oxford, UK: Oxford Science Publishers), 22 p.

Uncles, R. J. (2011). "Small-scale surface fronts in estuaries," in *Treatise on estuarine and coastal science* (Academic Press, Waltham), 53–74.

Zhou, M. Z. (2010). *Research on characteristics of circumfluence in zhoushan liuheng island (in chinese with english abstract)* (Zhejiang, China: Zhejiang University).